

Direct Detection Constraints on Dark Matter Event Rates in Neutrino Telescopes, and Collider Implications

Prateek Agrawal

Department of Physics, University of Maryland, College Park, MD 20742

Zackaria Chacko

Department of Physics, University of Maryland, College Park, MD 20742

Can Kilic

Department of Physics and Astronomy, Rutgers University, Piscataway NJ 08854

Rashmish K. Mishra

Department of Physics, University of Maryland, College Park, MD 20742

ABSTRACT: Neutrino telescopes are looking to detect neutrinos produced by the annihilation of weakly interacting massive particle (WIMP) dark matter in the sun. The event rate depends on the dark matter density in the sun, which in turn is dictated by the cross section of WIMPs with nucleons. This however is bounded by direct detection experiments. We use the constraints from these experiments to place model-independent upper bounds on the event rates in neutrino telescopes that apply to any elastic dark matter model. Since the spin-independent WIMP-nucleon cross section is much more tightly constrained than the corresponding spin-dependent cross section, the bounds are much stronger in the former case and are competitive with the current limits from IceCube. If the number of events observed in neutrino telescopes exceeds the upper bound corresponding to spin-independent interactions, the implication is that the cross section of dark matter with nucleons is dominated by spin-dependent interactions. In such a scenario the natural dark matter candidates are Majorana fermions and real vector bosons, so that dark matter particles are their own anti-particles. We show that any such theory that leads to observable event rates at current generation neutrino telescopes will in general contain new particles charged under the Standard Model gauge groups that naturally lie in a mass range that is kinematically accessible to the Large Hadron Collider (LHC).

1. Introduction

It is now well established that dark matter not contained in the Standard Model (SM) comprises about 80% of the total matter in the universe. However, the masses, spins and quantum numbers of the particles of which dark matter is composed are not known. One natural class of dark matter candidates are Weakly Interacting Massive Particles (WIMPs). These are stable particles with masses of order the weak scale that have weak scale cross-sections with visible matter. When the universe cools WIMPs naturally survive as thermal relics with the right relic abundance to explain observations. Many well-motivated extensions of the Standard Model contain WIMP dark matter candidates that have been shown to naturally give rise to the observed amount of dark matter, for example supersymmetry [1, 2], extra dimensional theories [3, 4], little Higgs models [5, 6, 7] and the left-right twin Higgs model [8].

How can WIMP dark matter be detected? In general, there are three classes of experiments which aim to detect WIMPs. These include

- direct detection experiments, which look for the recoil of nuclei after collisions with WIMPs,
- indirect detection experiments, which search for the annihilation products of WIMPs, and
- collider experiments, including the Large Hadron Collider (LHC), which hope to observe missing energy signatures associated with the direct production of WIMPs.

One promising class of indirect detection experiments involves neutrino telescopes, such as IceCube, which are looking to detect neutrinos produced by the annihilation of dark matter in the sun [9, 10]. This idea has been investigated in the context of models with supersymmetric dark matter (for example, [11, 12, 13, 14, 15, 16, 17], for a review see [18]), Kaluza-Klein dark matter [19, 20, 21, 22, 23], right-handed neutrino dark matter [24], little Higgs dark matter [25], the inert doublet model [26, 27, 28] and right-handed sneutrino dark matter [29]. The event rate in neutrino telescopes depends on the dark matter density in the sun, which in turn depends on the cross section for dark matter scattering off of nucleons. This however is bounded by recent direct detection experiments. The number of events that could be observed in neutrino telescopes is therefore highly correlated with the results of direct detection experiments [30, 31, 32, 33].

In this paper we use the constraints from direct detection experiments to place upper bounds on the possible event rates in neutrino telescopes that apply to any elastic dark matter model. These bounds can be parameterized as a function of the dark matter mass and of the branching ratios for WIMP annihilation into various SM final states. Since the spin-independent WIMP-nucleon scattering cross-section is much more tightly constrained than the corresponding spin-dependent cross-section, the bounds are much stronger in the former case. We find that the bounds corresponding to spin-independent interactions currently stand

at about a thousand events per year per km^2 for annihilation directly to neutrinos, and at a few hundred events per year per km^2 for annihilation into any other SM final states. For most final states, this is stronger than the current limits from IceCube [34, 35]. Furthermore, the upper bound on the event rate will go down to a handful of events a year if the direct detection limits improve by two orders of magnitude as expected. This is below the expected background from atmospheric neutrinos in neutrino telescopes. The bounds on the event rates arising from direct detection constraints on spin-dependent interactions, on the other hand, currently stand at the level of a few hundred thousand events per year. Therefore even with expected improvements in the near future, bounds corresponding to spin-dependent interactions will continue to be much weaker than the current limits from IceCube.

If the number of events observed in neutrino telescopes exceeds the upper bounds corresponding to spin-independent interactions, the implication is that the cross-section of dark matter with nucleons is dominated by spin-dependent interactions. A model-independent classification of dark matter candidates that have this property, based on the spin and quantum numbers of both the WIMP and the intermediate particle whose exchange mediates the WIMP-nucleon interaction, has been performed [36]. From this study, all theories that lead to elastic spin-dependent WIMP-nucleon scattering at tree-level through renormalizable interactions have been identified. It has been established that in such a scenario, the natural dark matter candidates are Majorana fermions and real vector bosons, so that the dark matter particle is its own anti-particle. Scalar and complex vector boson dark matter candidates are disfavored. Dirac fermions are also disfavored, unless the dark matter particle carries very specific quantum numbers. Furthermore, it has been shown that all renormalizable theories with primarily spin-dependent WIMP-nucleon cross sections at tree-level predict either

- new particles at the weak scale with Standard Model quantum numbers, or
- a Z' gauge boson with a weak scale mass that serves as a mediator.

In this paper we show that in the region of parameter space that is accessible to IceCube, these particles naturally lie within the mass range that is kinematically accessible to the LHC.

From this discussion we see that there is a very close connection between direct detection experiments, dark matter searches in neutrino telescopes and the LHC. A null result in the current generation of direct detection experiments, in association with a positive signal at IceCube, would constitute evidence that dark matter is composed of either Majorana fermions or real vector bosons, and therefore that dark particles are their own anti-particles. Furthermore, this conclusion would then very likely be confirmed by discoveries at the LHC.

The layout of the paper is as follows. In section 2 we give a brief overview of the relation between bounds from direct detection experiments and event rates at neutrino telescopes, for both spin-independent as well as spin-dependent WIMP-nucleon interactions. In section 3, we consider the models that give rise to primarily spin-dependent WIMP-nucleon interactions, and examine the parameter space of these theories that gives rise to an observable signal at

IceCube. We show that the masses of the new particles naturally lie in a region which is within the energy reach of the LHC. We conclude in section 4.

2. Correlating Direct Detection Experiments and Event Rates in Neutrino Telescopes

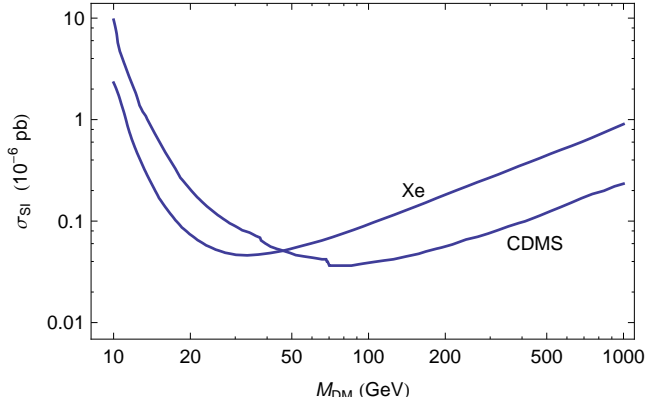
2.1 Bounds on WIMPs from Direct Detection Experiments

Direct detection experiments are designed to observe the recoil of a heavy nucleus when a WIMP scatters off it. The typical energy transfer is of order 10 keV, much smaller than the characteristic nuclear energy scales. Therefore in such an experiment the WIMP interacts with the entire nucleus as a single unit, with a net mass, charge and spin.

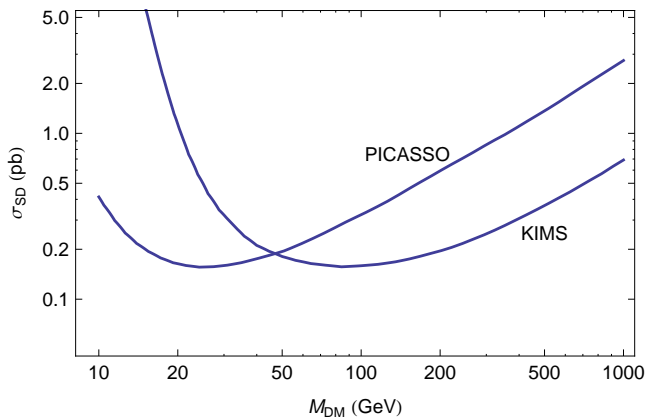
The cross-section for WIMPs to scatter off different nuclei depends strongly on the form of the interactions of the dark matter particle. In some cases the WIMP-nucleus cross-section is not sensitive to the spin of the nucleus, and we refer to such interactions as spin-independent. In other cases the WIMP couples dominantly to the spin of the nucleus, and we refer to such interactions as spin-dependent. The bounds on WIMP-nucleus scattering from direct detection experiments are generally expressed as limits on the WIMP-nucleon cross-section, allowing results across experiments using different nuclei to be compared.

The bounds from direct detection experiments on spin-dependent interactions are relatively weak since the spin of a typical nucleus is either zero or order one, and does not scale with A , the number of nucleons. Depending upon whether the unpaired nucleon in the nucleus is a proton or a neutron, a given experiment will in general place a bound only on the spin-dependent WIMP cross-section with either the proton or the neutron. On the other hand, spin-independent cross-sections are enhanced by a factor of A^2 , and the bounds on such interactions are correspondingly stronger by a factor of order 10^5 . In generating the spin-independent limits an implicit assumption is made that the WIMP scattering cross section off protons and neutrons is approximately the same, and that there are no large cancellations arising from interference between the amplitudes for scattering off protons and neutrons.

In Fig 1 we show current bounds for the spin-independent and spin-dependent WIMP-nucleon scattering cross sections. As we shall explain below, for our purposes only the bound on the spin-dependent WIMP-proton cross-section matters, and the bound on spin-dependent WIMP-neutron cross-section is irrelevant. The CDMS [37] and Xenon [38] experiments currently put the most stringent bounds on spin-independent scattering. For spin-dependent interactions on the other hand, the PICASSO [39] and KIMS [40] collaborations currently place the tightest bounds on the WIMP-proton cross-section. As is clear from the figures, bounds on spin-dependent scattering are much weaker, generally by more than five orders of magnitude. In the next sub-section we will translate these limits on the WIMP-nucleon cross section into an upper bound on WIMP capture rates in the sun, and from this into an upper bound on event rates in neutrino telescopes.



(a)



(b)

Figure 1: Current direct detection bounds on the a) spin-independent dark matter-nucleon cross section and b) the spin-dependent dark matter-proton cross section

2.2 Capture and Annihilation of Dark Matter in the Sun

As WIMPs pass through the sun, they are expected to scatter off the nuclei in the sun and become gravitationally bound. With subsequent scattering, they eventually accumulate in the center of the sun. These WIMPs eventually annihilate into various SM final states. The subsequent decays of these states generally result in high-energy neutrinos, which can be observed in neutrino telescopes here on earth.

Both spin-independent as well as spin-dependent scattering can lead to the capture of dark matter in the sun. Of the nuclei that have a net spin, hydrogen is the only one that is present in the sun in significant proportions. Other trace elements in the sun generally have no net spin, and even when they do, there is no A^2 enhancement that can compensate for

their low density fraction. Therefore, the only relevant quantity for spin-dependent capture is the WIMP-proton cross section. Spin-independent capture on the other hand receives contributions from several elements. As explained in the previous sub-section, the cross section for spin-independent WIMP-nucleus scattering is strongly enhanced by large A . For WIMP masses significantly larger than the mass of the nucleus, the inclusion of kinematic factors causes the WIMP-nucleus cross section to scale roughly as $\sim A^4$. Therefore, even though the heavier elements in the sun are rarer, this enhancement makes their contribution to the capture rate significant. In particular, as noted in [41], oxygen plays the most important role in spin-independent capture of WIMPs in the sun. We plot the contribution of some representative elements to the capture rate in Fig. 2. These numbers were obtained by using the software DarkSusy [42]. We see clearly that heavier elements cannot be neglected, and in fact may contribute significantly more to capture than either hydrogen or helium.

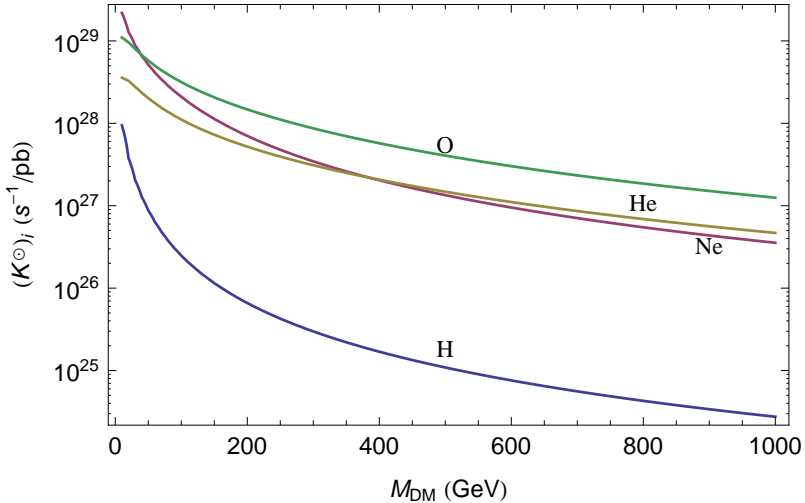


Figure 2: Contribution of various elements to the spin-independent capture rate in the sun

We present approximate analytical formulae for the capture rate to understand the dependence on various parameters. The spin-dependent capture rate in the sun is given by [18, 24],

$$C_{SD}^{\odot} \simeq 1.3 \times 10^{29} \text{ s}^{-1} \left[\frac{\rho_{local}}{0.3 \text{ GeV/cm}^3} \right] \left[\frac{270 \text{ km/s}}{\bar{v}_{local}} \right] \left[\frac{\sigma_{H,SD}}{1 \text{ pb}} \right] \left[\frac{1 \text{ GeV}}{m_{DM}} \right] S(m_{DM}/m_H) \quad (2.1)$$

$$\equiv K_{SD}^{\odot} \sigma_{SD}.$$

Here, $\sigma_{H,SD} = \sigma_{SD}$ is the spin-dependent cross section with hydrogen. The astrophysical parameters ρ_{local} and \bar{v}_{local} are the local halo density and root mean square velocity of the dark matter particles, and the numbers in the formula represent typical values. Finally, since the capture relies on the final dark matter particle being gravitationally bound, there is a kinematic suppression $S(m_{DM}/m_H)$ which depends on the ratio of the WIMP mass to the

mass of hydrogen. The function $S(x)$ approaches 1 for $x \rightarrow 1$, which corresponds to no suppression. On the other hand, if the WIMP is much heavier than hydrogen ($x \rightarrow \infty$), then $S(x) \propto x^{-1}$ while $S(x) \propto x$ for $x \rightarrow 0$.

The spin-independent capture rate, on the other hand, is a sum over contributions from various elements, and depends on the details of their relative compositions and distributions in the sun

$$\begin{aligned} C_{\text{SI}}^{\odot} &\simeq 4.8 \times 10^{22} \text{s}^{-1} \left[\frac{\rho_{\text{local}}}{0.3 \text{ GeV/cm}^3} \right] \left[\frac{270 \text{ km/s}}{\bar{v}_{\text{local}}} \right] \left[\frac{1 \text{ GeV}}{m_{\text{DM}}} \right] \\ &\quad \times \sum_i F_i(m_{\text{DM}}) f_i \phi_i S(m_{\text{DM}}/m_{N_i}) \left[\frac{1 \text{ GeV}}{m_{N_i}} \right] \left[\frac{\sigma_{N_i, \text{tot}}}{10^{-6} \text{ pb}} \right] \quad (2.2) \\ &\equiv K_{\text{SI}}^{\odot} \sigma_{\text{SI}}. \end{aligned}$$

Here the approximation that the WIMP-proton and WIMP-neutron cross sections are approximately equal has been used to go from the WIMP-nucleus cross section ($\sigma_{N_i, \text{tot}}$) to the WIMP-nucleon cross section (σ_{SI}). We now explain the significance of the various factors appearing in this equation. The dimensionless quantity f_i corresponds to the relative abundance of the elements in the sun. Hydrogen and helium are the most abundant elements in the sun ($f_H = 0.772$ and $f_{He} = 0.209$). For all other elements $f_i \sim 10^{-3}$. The effect of the different spatial distributions of various elements within the sun is accounted for by the dimensionless parameter ϕ_i . It is approximately equal for various elements in the sun $\phi_i \sim 3.2$, up to corrections of order a few percent. When the dark matter particle scatters off heavier nuclei, there is a form factor suppression because the WIMP probes only a part of the entire nucleus. The form factor F_i starts becoming significant for elements with $A > 20$. Finally, since the capture relies on the final dark matter particle being gravitationally bound, there is again a kinematic suppression $S(m_{\text{DM}}/m_N)$ when the dark matter mass and the nuclear mass differ. The exact details of this calculation may be found in [18].

The factors K^{\odot} are plotted as a function of the dark matter mass in Fig 3, for both the spin-independent and spin-dependent cases. This calculation was performed using Dark-Susy [42]. We can see from this that spin-independent WIMP-nucleon scattering is around two to three orders of magnitude more efficient in capturing dark matter than the corresponding spin-dependent scattering.

The number of dark matter particles (N) in the sun is governed by the simple equation,

$$\begin{aligned} \dot{N} &= C^{\odot} - 2\Gamma_A \\ &= C^{\odot} - A^{\odot} N^2. \end{aligned} \quad (2.3)$$

The quantity Γ_A which represents the WIMP annihilation rate depends on the parameter A^{\odot} which in turn depends on the annihilation cross section and the effective volume of the core

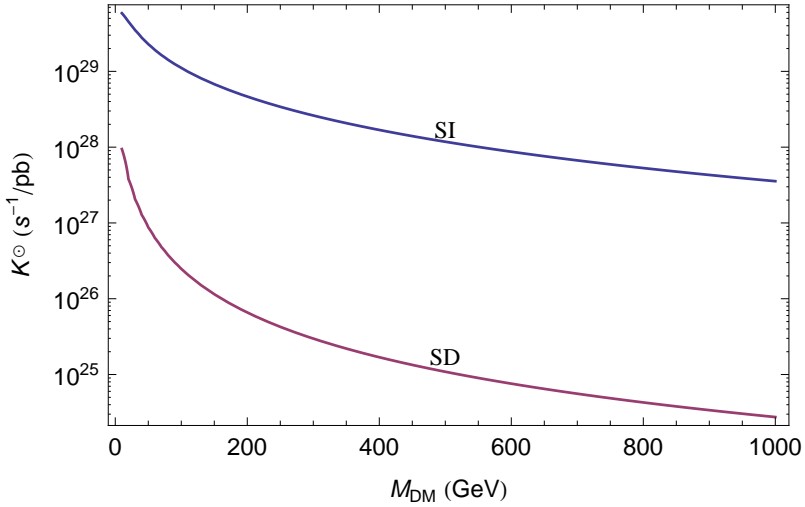


Figure 3: Capture “efficiency” in the sun for spin-independent and spin-dependent scattering

of the sun, V_{eff} ,

$$A^{\odot} = \frac{\langle \sigma v \rangle}{V_{\text{eff}}} \quad (2.4)$$

$$V_{\text{eff}} = 1.8 \times 10^{26} \text{ cm}^3 \left(\frac{1000 \text{ GeV}}{m_{DM}} \right)^{3/2}. \quad (2.5)$$

We can solve this equation to obtain the number density today, at $t_{\odot} \simeq 4.5$ billion years

$$N = \sqrt{\frac{C^{\odot}}{A^{\odot}}} \tanh \left(\sqrt{C^{\odot} A^{\odot}} t_{\odot} \right). \quad (2.6)$$

If the argument of the tanh function is large enough, the implication is that the process of capture and annihilation in the sun have come into equilibrium. This happens if the capture and annihilation cross sections are large enough to satisfy $\sqrt{C^{\odot} A^{\odot}} t_{\odot} > 1$. In this case the annihilation rate is equal to half the capture rate.

We plot the condition on the scattering and annihilation cross sections for dark matter to be in equilibrium in Fig 4. It is clear from the figure that for s-wave annihilation the condition for equilibration is always realized in any region of parameter space which yields an interesting signal in km^3 neutrino telescopes.

For annihilation into any given final state, the total annihilation rate Γ dictates the total number of high energy neutrinos produced. The maximum value of Γ depends only on the capture rate C^{\odot} . The capture rate in turn is proportional to the WIMP-nucleon scattering cross section, which is constrained by direct-detection experiments. Therefore the bounds from direct detection lead directly to an upper bound on the number of high energy neutrinos produced by WIMP annihilation in the sun into any specific SM final state. In the next subsection we will translate this into an upper bound on event rates in neutrino telescopes.

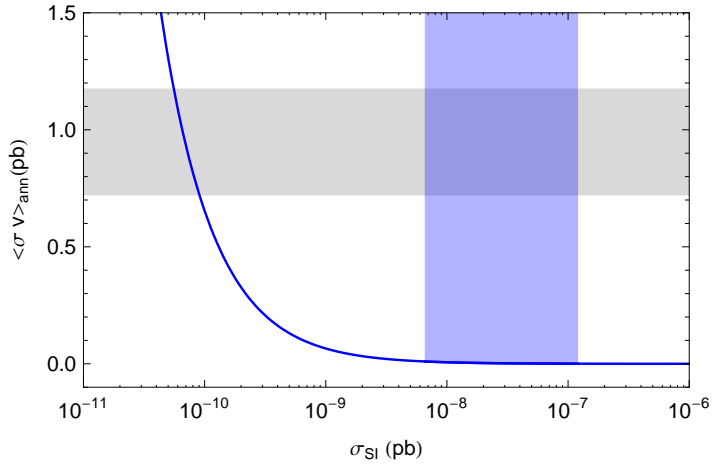


Figure 4: Equilibrium of dark matter capture/annihilation in the sun for mass $m_{DM} = 500$ GeV. The region above the curve ensures equilibrium. The parameter space to the right of the vertical shaded region has already been ruled out by direct detection experiments for spin-independent interactions. The region to the left of the vertical shaded region will generate fewer than 10 events per year per km^2 in neutrino telescopes (assuming a $\nu_\tau \bar{\nu}_\tau$ final state with $E_{th} = 10$ GeV). The horizontal shaded band indicates the annihilation rate required to be consistent with relic density observations assuming s-wave annihilation.

2.3 Upper Bound on Event Rates in Neutrino Telescopes

Neutrino telescopes are large $\sim \text{km}^3$ arrays of Cerenkov detectors placed inside a transparent medium such as ice or water. Energetic neutrinos from the sun interact with nucleons in the rock below the detector, and produce muons via charged current interactions. As these upward going muons propagate through the detector, they emit Cerenkov radiation, which is detected by the experiment.

The probability that a muon neutrino of energy E_ν produces an observable muon is given by

$$P(E_\nu, E_{th}) = N_A \sigma_{\nu N}(E_\nu) \langle R(E_\nu; E_{th}) \rangle, \quad (2.7)$$

where $\langle R(E_\nu; E_{th}) \rangle$ corresponds to the average range of the muons produced by neutrinos of energy E_ν before their energy drops below E_{th} , the energy threshold of the detector [43]. The average is over the fraction of energy carried by the muon,

$$\langle R(E_\nu; E_{th}) \rangle = \frac{1}{\sigma_{\nu N}(E_\nu)} \int_0^{1-E_{th}/E_\nu} dy R(E_\nu(1-y), E_{th}) \frac{d\sigma_{\nu N}}{dy}(E_\nu, y). \quad (2.8)$$

Here $\sigma_{\nu N}(E_\nu)$ is the neutrino-nucleon charged current interaction cross section [44] and $(1-y)$ is the fraction of neutrino energy carried off by the muon. The definition of the range used

here includes the density of standard rock and is measured in ‘kilometer water equivalents’ (*kmw.e.*) or equivalently, g/cm^2 .

The flux of muon-events observed is then given by [45, 44],

$$\Phi_\mu = \int \frac{d\phi_\nu}{dE_\nu} P(E_\nu, E_{th}) dE_\nu \quad (2.9)$$

$$= \int \int \frac{d\phi_\nu}{dE_\nu} \frac{d\sigma_{\nu N}}{dy} (E_\nu, y) N_A R(E_\nu(1-y), E_{th}) dy dE_\nu, \quad (2.10)$$

where N_A is Avogadro’s number. Here the differential flux of muon neutrinos arising from the various final states F is given by

$$\frac{d\phi_\nu}{dE_\nu} = \sum_F B_F \frac{\Gamma_A}{4\pi d^2} \frac{dN_\nu^F}{dE_\nu}, \quad (2.11)$$

where B_F is the branching fraction into the final state F , Γ_A is the annihilation rate, d is the distance of the sun from earth and dN_ν^F/dE_ν is the energy spectrum of muon-neutrinos produced in the sun from annihilation into the final state F .

If the threshold energy can be neglected compared to the neutrino energy, the range of the muon is approximately proportional to the muon energy. The charged-current cross section turns out to be proportional to the neutrino energy when the neutrino energy is of $\mathcal{O}(\text{TeV})$. In this case, we can rewrite the above expression,

$$\Phi_\mu = \sum_F B_F \frac{\Gamma_A}{4\pi d^2} \int \frac{dN_\nu^F}{dE_\nu} E_\nu^2 dE_\nu \int_0^1 N_A \frac{1}{E_\nu} \frac{d\sigma_{\nu N}}{dy} (E_\nu, y) \frac{R(E_\nu(1-y); 0)}{E_\nu} dy. \quad (2.12)$$

With this approximation, the second integral is independent of the neutrino energy, and can be numerically estimated for a given detector. Therefore the number of events observed is proportional to the quantity $\langle Nz^2 \rangle$, defined as,

$$\langle Nz^2 \rangle_F(m_{\text{DM}}) \equiv \frac{1}{m_{\text{DM}}^2} \int \frac{dN_\nu^F}{dE_\nu} E_\nu^2 dE_\nu. \quad (2.13)$$

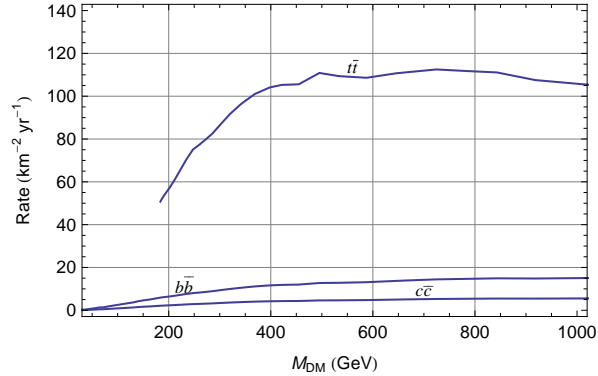
The total rate in the detector is given by the sum of the rate for muons and the corresponding rate for anti-muons,

$$\Phi_{tot} = \Phi_\mu + \Phi_{\bar{\mu}}. \quad (2.14)$$

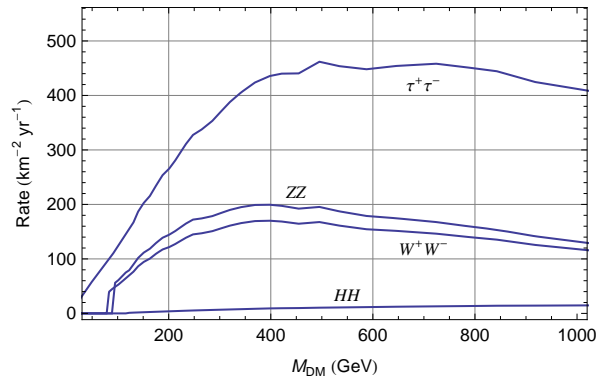
We can then write the total event rate in an empirical form,

$$\Phi_{tot} = (2.54 \times 10^{-23} \text{ km}^{-2} \text{ yr}^{-1}) \left(\frac{\Gamma_A}{s^{-1}} \right) \left(\frac{m_{\text{DM}}}{1 \text{ GeV}} \right)^2 \sum_{i=\nu, \bar{\nu}} a_i b_i \sum_F B_F \langle Nz^2 \rangle_F(m_{\text{DM}}). \quad (2.15)$$

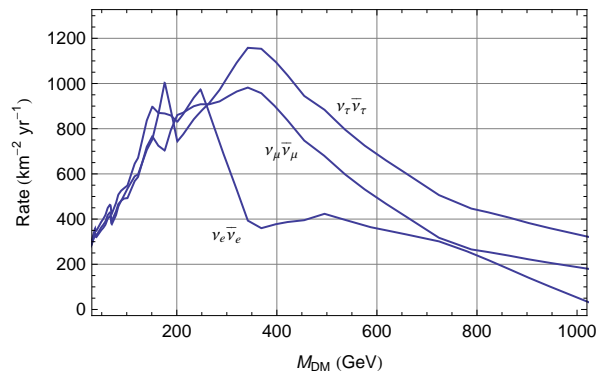
where the a_i are scattering coefficients for neutrinos and anti-neutrinos, which take values $a_\nu = 6.8$ and $a_{\bar{\nu}} = 3.1$, while the b_i are the range coefficients for muons and anti-muons, with values $b_\nu = 0.51$ and $b_{\bar{\nu}} = 0.67$.



(a)

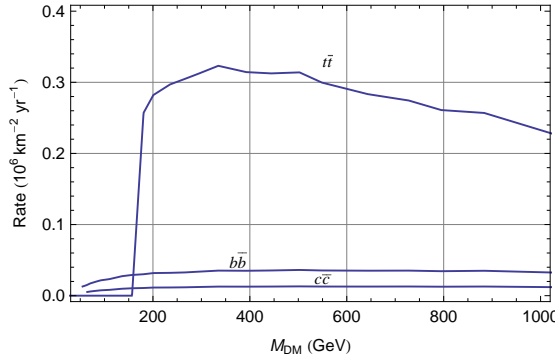


(b)

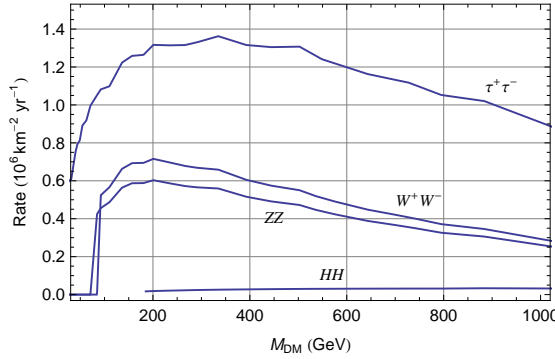


(c)

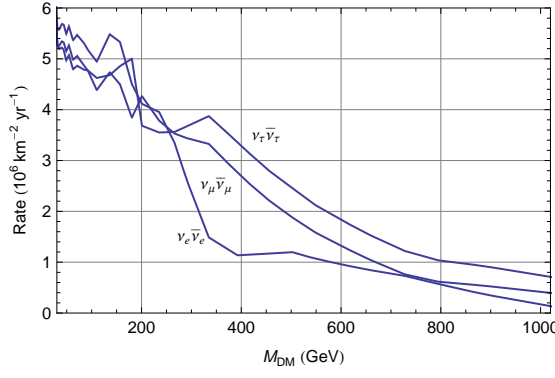
Figure 5: Maximum event rate in a neutrino detector consistent with direct detection bounds from spin-independent dark matter for various final states. The threshold energy was chosen to be $E_{th} = 10$ GeV.



(a)



(b)



(c)

Figure 6: Maximum event rate in a neutrino detector consistent with direct detection bounds from spin-dependent dark matter for various final states. The current experimental bounds from IceCube and Super-Kamiokande are much stronger. The threshold energy was chosen to be $E_{th} = 10$ GeV.

In this expression, the effects of neutrino propagation and detector thresholds have been neglected. For a relatively heavy WIMP ignoring detector threshold effects may be justified because the neutrino (and hence the muon) energies are typically higher than the detector threshold (for IceCube, $E_{\text{th}} \simeq 10$ GeV). Further, since the detection rate depends on the second moment of the neutrino spectrum, it is dominated by high energy neutrinos. Nevertheless, for a complete determination of the signal, the effects of neutrino propagation and the detector threshold must be folded in to the above expression. In order to estimate their impact on these formulas, we use results from the package DarkSusy [42]. We find that these effects are not insignificant for certain final states, and can change the answer by as much as 50%. Therefore, the formulae obtained above should only be used as a qualitative guide.

We are now in a position to determine the maximum event rate in neutrino telescopes. We set the WIMP-nucleon scattering cross section to its upper bound, as determined by the CDMS experiment for spin-independent scattering and by the KIMS experiment for spin-dependent scattering. We can then determine the muon flux at the neutrino telescope and we plot the result as a function of the WIMP mass for various neutrino-rich two body SM final states that the WIMPs annihilate into. This gives us the maximum possible signal rates in neutrino telescopes consistent with direct detection experiments, assuming that the WIMP has either purely spin-independent interactions (results plotted in Fig 5), or purely spin-dependent interactions (results plotted in Fig 6). In obtaining the results for annihilation to two Higgs particles, we have assumed a Higgs mass of 120 GeV. As noted above, our formulae do not include (potentially important) threshold and neutrino propagation effects. Therefore, we plot the results obtained from DarkSusy.

We see from these figures that models with spin-independent interactions do not generate more than about 500 events per year per km^2 in neutrino detectors, unless annihilation occurs directly to neutrinos, in which case the rate can be as large as 1200 events per year per km^2 . Note that if dark matter is composed of scalars or Majorana fermions, annihilation into a neutrino-antineutrino pair is highly disfavored from angular momentum considerations. For all final states except neutrinos, these bounds are comparable to or stronger than the corresponding limits from IceCube. The current generation of direct detection experiments [46], [47] have the potential to strengthen this bound by an additional two orders of magnitude. In such a scenario the maximum number of events will be reduced well below the background from atmospheric neutrinos, and the spin-independent case will go out of reach of current generation neutrino telescopes. We also see from the figures that the corresponding bounds on the event rates for models with purely spin-dependent interactions are much weaker, and are not competitive at all with the current limits from neutrino telescopes.

In Fig 7 we plot the current IceCube [34] and Super-Kamiokande [48] bounds on the event rates assuming annihilation to the W^+W^- final state, together with bounds on the event rate from direct detection experiments. It is clear from these plots that the direct detection bounds on spin-independent interactions lead to a tighter constraint on event rates

than the current IceCube limit. With the operation of newer detectors, the spin-independent bound will only become stronger, and consequently is expected to be beyond the reach of IceCube 5 year sensitivity [49]. The spin-dependent case, on the other hand, is seen to allow a much higher flux. In fact, by far the strongest bound on the spin-dependent interaction (assuming W^+W^- annihilation) is seen to come from IceCube.

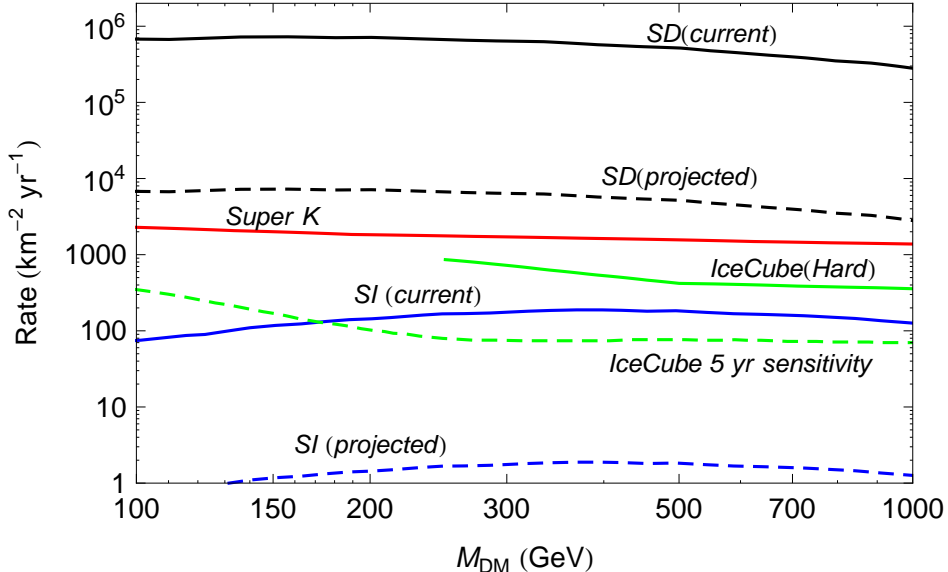


Figure 7: Shown are bounds and projected bounds on the event rate from Super Kamiokande and IceCube. Also plotted are limits on the event rate obtained from null results in direct detection experiments, both at present and projected (two orders of magnitude stronger). Solid lines denote current bounds and dashed lines denote projections. The final state was assumed to be W^+W^- and the threshold energy set at 1 GeV.

If the number of events observed in neutrino telescopes were to exceed the upper bounds corresponding to spin-independent interactions, the implication is that the cross section of dark matter with nucleons is dominated by spin-dependent interactions. In the next section, we consider the dark matter models that have this property. However, before we do so, we briefly consider the effect of relaxing some of the assumptions that went into obtaining these bounds.

- We restricted ourselves to WIMP annihilations into two particle SM final states. Relaxing this assumption by allowing multi-body SM final states does not affect the upper bound. The reason is that for any given WIMP mass, the neutrinos arising from the decays of a multi-particle final state each carry correspondingly less energy. Since the neutrino-nucleus cross section scales as the energy of the incident neutrino, as does the range of the muon produced in the collision, these effects reduce the signal more than

enough to compensate for the increased number of neutrinos.

- We did not consider the possibility of annihilations into non-SM final states composed of new particles yet to be discovered. These could subsequently decay into SM states and eventually into neutrinos, thereby generating a signal. However, we do not expect this to alter the upper bound, since each SM particle will carry less energy than if annihilation had occurred directly to two SM particles, with a corresponding reduction in the signal.
- We ignored effects like Sommerfeld enhancement [50, 51, 52, 53], which can significantly affect the annihilation rate. This is justified because the upper bound on the signal is controlled only by the capture rate, and does not depend on the annihilation rate.
- We assumed a specific value for the local halo density. Our bounds on the event rates are insensitive to this value since it affects the capture rate and the direct detection bounds in exactly the same way.
- We assumed a specific distribution of dark matter velocities. The result is in fact sensitive to this assumption since it affects the capture rate and the direct detection bounds somewhat differently. However, we do not expect the uncertainties in this to affect our conclusions significantly.
- We restricted our considerations to elastic dark matter. Our result does not apply to inelastic dark matter [54, 55, 56] or more generally to any type of form-factor dark matter [57, 58, 59] since the relationship between the capture rate and the direct detection bounds is now modified [60, 61].
- Finally, note that in obtaining these bounds we have not restricted ourselves to thermal dark matter, but have also allowed for the possibility that dark matter is composed of non-thermal WIMPs.

3. Collider Implications

In this section we consider the implications for the LHC if the WIMP-nucleon spin-dependent cross-section lies within the parameter space that will be probed by IceCube. The dark matter candidates that can naturally give rise to primarily spin-dependent interactions in a renormalizable theory have been classified [36], and the results are shown in Table 1. From the table it is clear that if the interactions of WIMPs with nucleons are primarily spin-dependent, the natural dark matter candidates are either Majorana fermions or real vector bosons. Furthermore, corresponding to each dark matter candidate, the spins and quantum numbers of the particles mediating the tree-level spin-dependent WIMP-nucleon interaction are also constrained. In this section we study the range of masses of the dark matter particle, and also of the mediating particle, that lead to an observable signal from spin-dependent

Dark Matter	Mediator	Process	Scattering
Scalar	Z, Z'		SI
	h		SI
	Q		SI
Dirac Fermion	Z, Z'		SI, SD [†]
	h		SI
	X		SI, SD
	Φ		SI, SD
Majorana Fermion	Z, Z'		SD
	h		SI
	X		SD in chiral limit
	Φ		SD in chiral limit
Real Vector	h		SI
	Q		SD in chiral limit
Complex Vector	Z, Z'		SI
	h		SI
	Q		SI, SD

Table 1: A summary of results for WIMP-nucleon scattering, for each dark matter candidate and mediator [36]. In the Feynman diagrams, scalars are represented by dashed lines, fermions by solid lines and vector bosons by wavy lines. Of the mediators, h , Z' and the SM Z are neutral under both electromagnetism and color, while X , Φ and Q transform as triplets under color and carry electric charge.

[†]Can be primarily SD for specific choices of Z' charges

	proton	neutron
Δ_u	0.78 ± 0.02	-0.48 ± 0.02
Δ_d	-0.48 ± 0.02	0.78 ± 0.02
Δ_s	-0.15 ± 0.02	-0.15 ± 0.02

Table 2: Quark spin fraction in the proton and neutron [62, 63]

interactions at IceCube. We will establish that these particles naturally tend to lie within the energy range that will be probed by the LHC. Our approach will be to study the various candidate theories in turn, and study the range of particle masses in each case.

3.1 Majorana Fermion

The effective operator that gives rise to spin-dependent scattering in this case can be shown to be

$$L_{\text{eff}} = d_q \bar{\chi} \gamma^\mu \gamma^5 \chi \bar{q} \gamma_\mu \gamma^5 q, \quad (3.1)$$

where χ is the Majorana spinor corresponding to the dark matter particle and q represents a quark field. The corresponding WIMP-nucleus cross-section is given by

$$\sigma_0 = \frac{16m_\chi^2 m_N^2}{\pi(m_\chi + m_N)^2} \left[\sum_{q=u,d,s} d_q \lambda_q \right]^2 J_N(J_N + 1). \quad (3.2)$$

For scattering off a free nucleon $\lambda_q = \Delta_q^n$. The quantities Δ_q are the spin-fraction of the nucleon spin carried by quark q , listed in Table 2. J_N is the angular momentum of the nucleus, and is equal to $\frac{1}{2}$ for free nucleons.

We see from the table that if dark matter is composed of Majorana fermions, spin-dependent WIMP-nucleon scattering can arise through any of

- t-channel vector exchange,
- s- and u-channel vector exchange, or
- s- and u-channel scalar exchange

If the process occurs via the s or u-channels the mediating particle necessarily carries SM color. For a t-channel process the mediating vector boson may either be the SM Z , or a new Z' . If it is the SM Z , the dark matter particle carries weak charge. Therefore we see that each of these processes is associated either with a new particle charged under the SM gauge groups, or with a new Z' gauge boson.

The values of d_u , d_d and d_s which appear in equation (3.2) depend on the flavor structure of the underlying theory, and must be consistent with constraints on flavor-violating processes.

Dark matter scattering mediated by a Z' will automatically satisfy these constraints provided that the couplings of the Z' are flavor diagonal. This implies that in these models $d_d = d_s$. For theories where WIMP-nucleon scattering is mediated by X_μ or Φ , the flavor structure is more complicated. In general, a GIM mechanism which incorporates either multiple flavors of the dark matter particle or multiple flavors of the mediators is required in order to ensure that flavor bounds are satisfied. For concreteness, in what follows we assume that there are multiple mediators. Flavor bounds are then satisfied provided that the mediators corresponding to different flavors are quasi-degenerate and their couplings are flavor-diagonal.

t-channel vector exchange

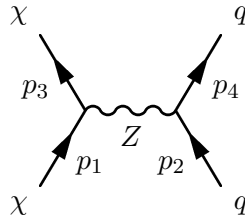


Figure 8: Majorana dark matter scattering through t-channel vector exchange

We begin with t-channel exchange of a vector. The Lagrangian corresponding to this process can be written in four-component language as,

$$\mathcal{L} = -\frac{1}{4}\mathcal{F}^{\mu\nu}\mathcal{F}_{\mu\nu} + \frac{1}{2}m_Z^2 Z^\mu Z_\mu + \bar{\chi}\gamma^\mu(-\beta\gamma^5)\chi Z_\mu + \bar{q}\gamma^\mu(\tilde{\alpha} - \tilde{\beta}\gamma^5)q Z_\mu. \quad (3.3)$$

For simplicity, in this expression flavor indices have been suppressed. It is straightforward to verify that the coefficient of the effective operator defined in equation (3.1) is

$$d_q = -\frac{\beta\tilde{\beta}_q}{m_Z^2}. \quad (3.4)$$

Here Z could represent either the SM Z or a new Z' under which the SM matter fields are charged. For the Standard Model Z ,

$$d_u = -d_d = -d_s. \quad (3.5)$$

We choose to assign the Z' charges in the same way, because for a given WIMP-proton cross-section this choice of signs corresponds to the highest value of the mass of the exchanged particle, and is therefore the conservative assumption. It is also naturally consistent with flavor bounds on new physics, as noted above. The physics of the two cases is however very different, and so we consider them separately.

If the WIMP carries charge under the Z , it must either constitute the neutral component of a single SM $SU(2)_L$ representation or arise as a linear combination of the neutral components of different representations of $SU(2)_L$. Majorana fermion dark matter that arises from a single $SU(2)_L$ representation is very tightly constrained by direct detection experiments.

For example, Majorana neutrino dark matter has been excluded by Xenon in the mass range considered here [38]. We will therefore not consider this possibility further.

Although theories where the dark matter arises as a linear combination of the neutral components of different $SU(2)_L$ representations are also constrained by direct detection experiments, the bounds are significantly weaker. In general there are both spin-dependent WIMP-nucleon interactions arising from Z exchange as well as spin-independent interactions arising from Higgs exchange. The magnitudes of these two different contributions to the WIMP-nucleon cross section are not in general independent, but are correlated [64].

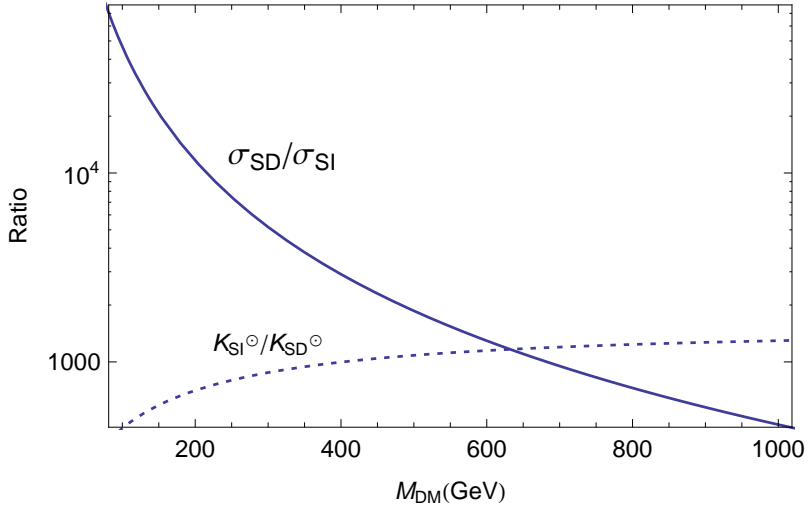


Figure 9: The ratio of spin-dependent and spin-independent cross-sections in the benchmark model for WIMP-nucleon scattering through the SM Z boson. We also show the ratio of capture efficiencies, $K_{SI}^\odot/K_{SD}^\odot$. To the left of the intersection, the neutrinos from SD interactions dominate.

To understand this correlation we work in the benchmark model of reference [36]. This model consists of two $SU(2)_L$ fermion doublets ξ and ξ^c which have equal and opposite hypercharges $Y = \pm \frac{1}{2}$. The dark matter particle arises as a linear combination of the neutral components of ξ and ξ^c . The mass matrix consists of a Dirac term linking ξ and ξ^c , together with a Majorana term that arises from a non-renormalizable interaction of the form $(H^\dagger \xi)^2$. When the SM Higgs doublet H gets a VEV, the neutral component of ξ acquires a Majorana mass. It also obtains a Yukawa coupling to the physical Higgs field h . Such a non-renormalizable operator may be generated by integrating out a SM singlet. The Lagrangian for the neutral components of ξ and ξ^c takes the form

$$\mathcal{L} \supset -\frac{g}{\cos \theta_W} \left(\bar{\xi}_0 \frac{1}{2} \bar{\sigma}^\mu \xi_0 - \bar{\xi}_0^c \frac{1}{2} \bar{\sigma}^\mu \xi_0^c \right) Z_\mu - \left[\frac{1}{2} \begin{pmatrix} \xi_0^c & \xi_0 \end{pmatrix} \begin{pmatrix} 0 & M \\ M & m \end{pmatrix} \begin{pmatrix} \xi_0^c \\ \xi_0 \end{pmatrix} + y_\xi \xi_0 \xi_0 h + \text{h.c.} \right]. \quad (3.6)$$

Here $y_\xi = m/v$ where $v = 246$ GeV is the electroweak VEV, and h is the physical Higgs field of the SM. The lighter of the two mass eigenstates ξ_D is the dark matter particle.

$$\xi_D = \cos \phi \, \xi_0 + \sin \phi \, \xi_0^c, \quad (3.7)$$

where ϕ is the mixing angle. The couplings to the Z and to the SM Higgs in the mass basis take the form,

$$\mathcal{L} \supset -\frac{g \cos 2\phi}{2 \cos \theta_W} \bar{\xi}_D \bar{\sigma}^\mu \xi_D Z_\mu - [y_\xi \cos^2 \phi \xi_D \xi_D h + \text{h.c.}] . \quad (3.8)$$

In terms of a four-component Majorana fermion χ , the Lagrangian becomes

$$\mathcal{L} \supset \frac{g \cos 2\phi}{4 \cos \theta_W} \bar{\chi} \gamma^\mu \gamma^5 \chi Z_\mu - y_\xi \cos^2 \phi \bar{\chi} \chi h. \quad (3.9)$$

In order to understand the correlation between the spin-dependent and spin-independent contributions to the WIMP-nucleon cross section let us estimate the mixing in the limit $m \ll M$. The coupling to the Z is suppressed by $\cos 2\phi$, which in this limit is simply $m/2M$, while the dark matter mass is approximately equal to M . On the other hand the coupling to the Higgs is proportional to m/v , where $v = 246$ GeV is the electroweak VEV. Therefore in this limit the ratio of the spin-dependent WIMP-nucleon cross section to the corresponding spin-independent cross section is fixed for any given value of M . We have plotted the ratio of these cross sections as a function of the WIMP mass in Fig 9, in the limit that the spin-independent cross section is at its current bound and assuming a Higgs mass of 120 GeV. Note that the spin-dependent cross section never exceeds the spin-independent cross section by more than a factor of about 10^5 for dark matter masses greater than 150 GeV. We have also shown on the same plot the ratio of capture efficiencies in the spin-independent and spin-dependent cases. Clearly, spin-independent capture dominates for WIMP masses larger than about 600 GeV. Therefore a limit on the spin-independent WIMP-nucleon cross section directly translates into an upper bound on the event rate in neutrino telescopes in this benchmark model. We expect that the same conclusion will apply to the more general class of models where spin-dependent scattering is mediated by the SM Z .

In Fig 10 we have plotted the current upper limit on the event rate from direct detection experiments in this scenario as a function of the dark matter mass, assuming annihilation is entirely to the W^+W^- final state. We have also shown the current and future experimental bounds from IceCube. Note that in this and subsequent plots we do not require that annihilation and capture are mediated by the same particle, but allow for the possibility that these are mediated by different particles. In particular, dark matter annihilation exclusively to W^+W^- is not possible if mediated by the SM Z . We see that a signal close to the present IceCube bound implies a dark matter mass less than about 400 GeV, which is promising for the LHC. More generally, in most of the parameter space that is within the 5-year sensitivity of IceCube, the dark matter particle and its charged partners ξ^+ and ξ^{c-} have masses below

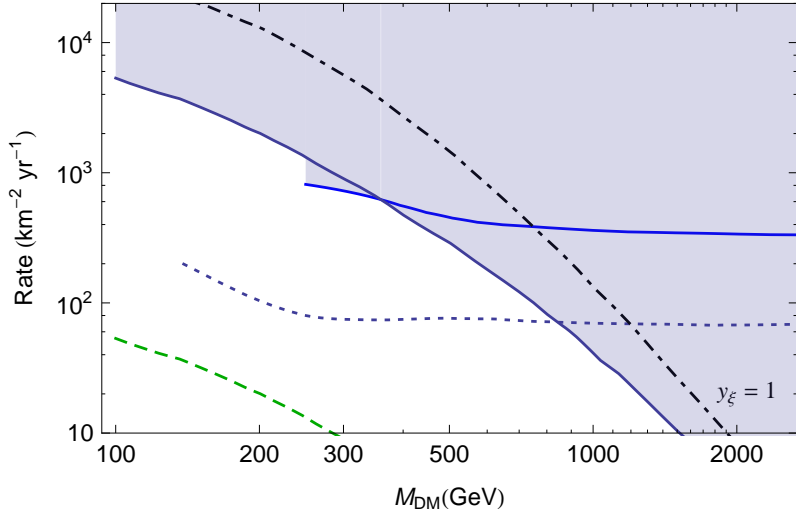


Figure 10: Estimates for the rates in IceCube for a Majorana dark matter coupling through the Standard Model Z , annihilating into W^+W^- ($E_{th} = 10$ GeV). The coupling was assumed to be at the CDMS spin-independent bound (blue solid line) and at a projected spin-independent bound (green dashed line). The IceCube current bound and 5 year sensitivity (dotted line) are also shown. The dot-dashed line corresponds to the WIMP-Higgs Yukawa coupling $y_\xi = 1$. The shaded region has been excluded by either direct detection experiments or IceCube.

1 TeV. The interesting region of parameter space lies below the line corresponding to $y_\xi = 1$, indicating that it is under perturbative control. In the same figure, we have also shown the effect on the event rate if the direct detection bounds improve by two orders of magnitude, as expected. In such a scenario, the signal in this class of theories would fall below the sensitivity of IceCube. Although this analysis has been performed for a specific benchmark model, we expect that similar conclusions hold in general for spin-dependent interactions mediated by the SM Z .

We now turn to the case of the Z' . There is now much more freedom with regard to charge assignments and the overall strength of the interaction. Also, there need not be a spin-independent contribution to the cross section from scalar exchange. However, experimental constraints on the masses and couplings of new Z' gauge bosons disfavor large event rates. As in the case of the SM Z , we set $d_u = -d_d = -d_s$, since this choice is naturally consistent with flavor constraints on new physics, and yields a conservative estimate for the mediator mass. The values β and $\tilde{\beta}$ equal to a $\frac{1}{2}$ correspond to chiral fermions having unit charge under the Z' . We use these as representative values. In Fig 14 we have shown the range of values of the Z' mass that would lead to a signal in neutrino telescopes at the current bound, or at the 5-year sensitivity. Unfortunately, a large portion of the allowed range of masses is disfavored by precision electroweak measurements and by bounds on direct production and four-point

interactions [65, 66], except perhaps for very specific Z' charge assignments.

s- and u-channel vector exchange

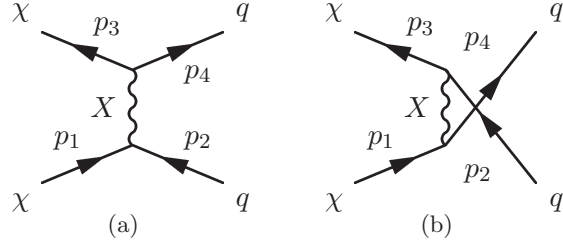


Figure 11: Majorana dark matter scattering through s- and u-channel vector exchange

We now move on to s- and u-channel exchange of a colored vector particle X . The Lagrangian corresponding to this process is

$$\mathcal{L} = -\frac{1}{2} |\partial_\mu X_\nu - \partial_\nu X_\mu|^2 + m_X^2 X_\mu^\dagger X^\mu + \bar{\chi} \gamma^\mu (\alpha - \beta \gamma^5) q X_\mu + \bar{q} \gamma^\mu (\alpha^* - \beta^* \gamma^5) \chi X_\mu^\dagger. \quad (3.10)$$

The co-efficient of the effective operator in this case is given by

$$d_q = -\frac{|\alpha_q|^2 + |\beta_q|^2}{2(m_{X,q}^2 - m_\chi^2)}. \quad (3.11)$$

In the chiral limit, the X vector bosons that couple to left- and right-handed quarks are in general distinct particles. In the absence of tuning, it is therefore natural for one of these two contributions to dominate. For the left-handed contribution, if the dark matter particle is a SM singlet then SM $SU(2)_L$ symmetry implies that $d_u = d_d$. Further, flavor constraints require $d_d = d_s$. Then the numerical values of Δ_u , Δ_d and Δ_s imply that there are large cancellations among the contributions of the different left-handed quarks to the WIMP-nucleon cross section, which is therefore somewhat suppressed. For the right-handed contribution, this cancellation can be avoided if $d_u \gg d_d (= d_s)$, or vice versa.

In figures 14 and 15 we have plotted the range of values of the X masses that would lead to a signal at IceCube, assuming annihilation to the W^+W^- final state (in general through a distinct set of mediators). In Fig 14 we have set $d_d = d_s = 0$ and $d_u \neq 0$, with $\alpha_u = -\beta_u = \frac{1}{2}$, corresponding to one natural possibility for the contribution from right-handed quarks. In Fig 15, on the other hand, we have set $d_u = d_d = d_s$, with $\alpha_q = \beta_q = \frac{1}{2}$ corresponding to the contribution from left-handed quarks. We see that away from the resonance region at $m_\chi = m_X$, the colored vector boson masses lie at a TeV or below in most of the parameter space. They are therefore kinematically accessible to the LHC, and can be pair-produced through strong interactions. They then decay, leading to a jets + missing energy signal. Recent model-independent studies of dark matter signals at the LHC involving jets + missing energy have been performed, for example, in [67, 68], [69], [70], and the results look promising.

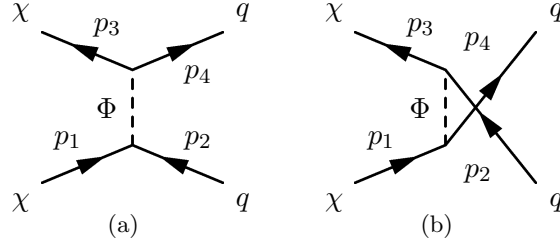


Figure 12: Majorana dark matter scattering through scalar exchange

s- and u-channel scalar exchange

Finally we consider scattering through s- and u-channel exchange of a colored scalar Φ . The Lagrangian corresponding to this process is

$$\mathcal{L} = |\partial\Phi|^2 - m_\Phi^2 |\Phi|^2 - \bar{\chi}(\alpha - \beta\gamma^5)q\Phi - \bar{q}(\alpha^* + \beta^*\gamma^5)\chi\Phi^\dagger. \quad (3.12)$$

The coefficient of the relevant operator is given by,

$$d_q = \frac{|\alpha_q|^2 + |\beta_q|^2}{4(m_{\Phi,q}^2 - m_\chi^2)}. \quad (3.13)$$

As explained earlier, in the chiral limit the mediators of left- and right-handed interactions are distinct. In figures 14 and 15 we have shown the range of values of the Φ mass that would lead to a signal at IceCube. In Fig 14 we have set $d_u \neq 0$ and $d_d = d_s = 0$, with $\alpha_u = -\beta_u = \frac{1}{2}$, corresponding to the right-handed contribution. In Fig 15 we have set $d_u = d_d = d_s$ with $\alpha_q = \beta_q = \frac{1}{2}$, corresponding to the left-handed contribution. We see that away from the resonance region the Φ masses lie below a TeV, which is promising for the LHC.

3.2 Vector Dark Matter

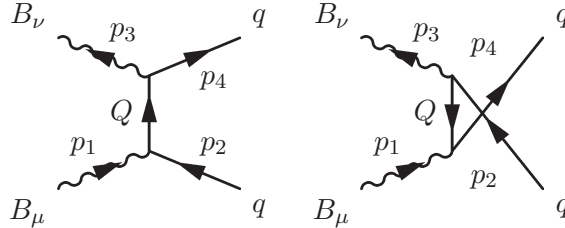
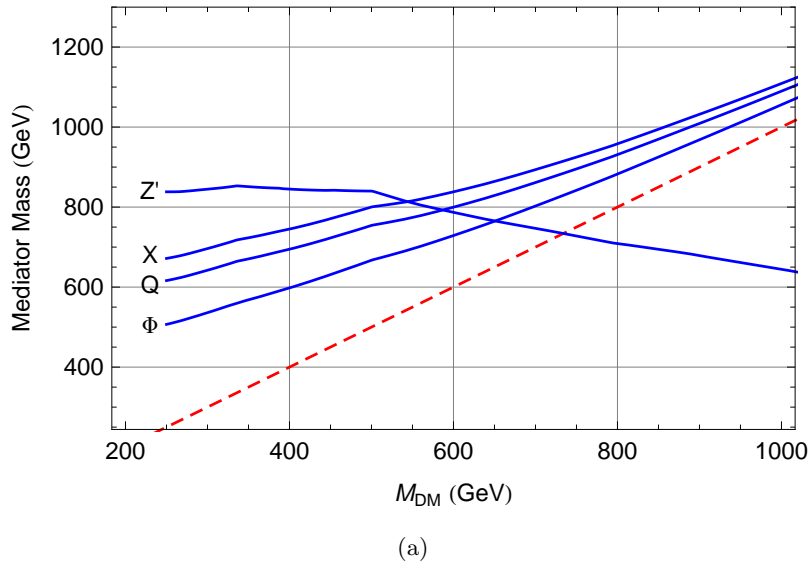


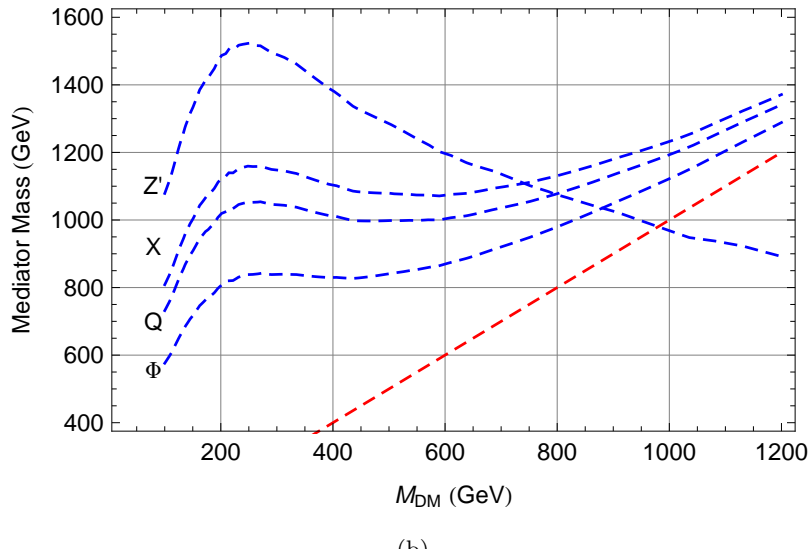
Figure 13: Vector dark matter scattering through s and u-channel fermion exchange.

The effective operator that generates spin-dependent scattering in the case that dark matter is a real vector field B_μ has the form

$$\mathcal{L} = b_q(\partial_\sigma B_\mu)B_\nu \bar{q}\gamma_\alpha \gamma^5 q \epsilon^{\sigma\mu\nu\alpha}. \quad (3.14)$$

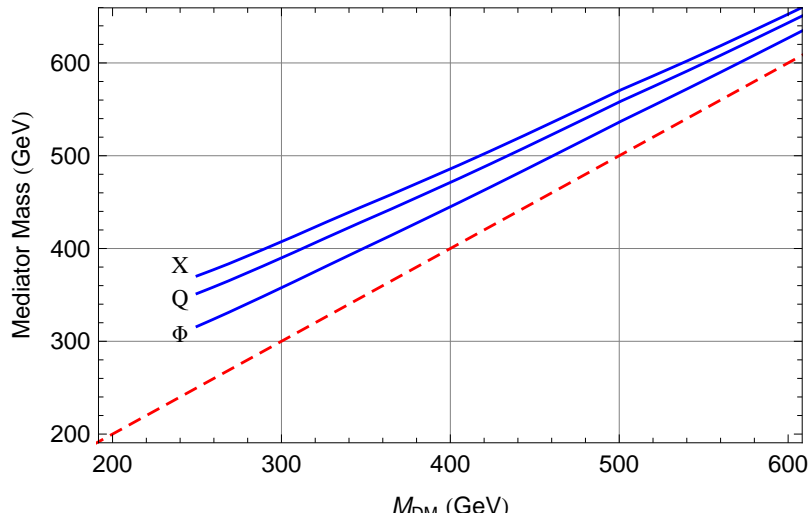


(a)

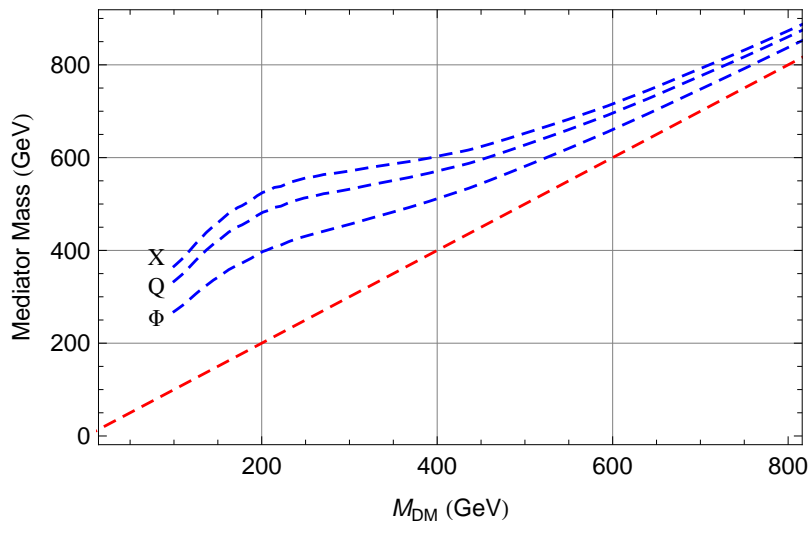


(b)

Figure 14: Estimates for the mediator masses if IceCube sees a signal near the present bound (above) or at the 5-year sensitivity (below). The colored mediators X , Φ and Q are assumed to couple only to up-type quarks, while the charges of the Z' are assumed to be proportional to the charges of the SM Z . The masses of X , Φ and Q must lie above the red dashed line, which corresponds to where the mediator mass is equal to the dark matter mass. The threshold energy was chosen to be $E_{th} = 10$ GeV.



(a)



(b)

Figure 15: Estimates for the colored mediator masses if IceCube sees a signal near the present bound (above) or at the 5-year sensitivity (below), assuming equal couplings to up- and down-type quarks. The signal in neutrino telescopes is suppressed due to cancellations arising from quark spin fractions, leading to lower values of the mediator masses. The threshold energy was chosen to be $E_{th} = 10$ GeV.

The corresponding WIMP-nucleus cross section is then

$$\sigma_0 = \frac{8m_\chi^2 m_N^2}{3\pi (m_\chi + m_N)^2} \left[\sum_{q=u,d,s} b_q \lambda_q \right]^2 J_N(J_N + 1). \quad (3.15)$$

This operator can be generated by the exchange of a heavy colored fermion Q in the s- and u-channels, as shown in Fig 13. The relevant part of the Lagrangian takes the form

$$\mathcal{L} = \bar{Q}(i\cancel{d} - m_Q)Q + \bar{q}\gamma^\mu(\alpha - \beta\gamma^5)Q B_\mu + \bar{Q}\gamma^\mu(\alpha^* - \beta^*\gamma^5)q B_\mu. \quad (3.16)$$

We find that

$$b_q = \frac{|\alpha_q|^2 + |\beta_q|^2}{(m_{Q,q}^2 - m_B^2)}. \quad (3.17)$$

We seek to explore the range of masses of the mediator Q and the dark matter particle B_μ that give rise to a signal at IceCube, and the resulting implications for the LHC. As in the cases of X and Φ , in the chiral limit the mediators Q that couple to left-and right-handed quarks are in general different particles, and the mediators corresponding to different flavors are also distinct. Flavor constraints are satisfied provided the mediators associated with different flavors are degenerate, and their couplings are flavor diagonal. For concreteness we employ exactly the same conventions as earlier. Specifically, we first consider $b_u \neq 0$, $b_d = b_s = 0$ with $\alpha_u = -\beta_u = \frac{1}{2}$, corresponding to the contribution from right-handed quarks. The results are plotted in Fig 14. We then consider $b_u = b_d = b_s$ with $\alpha_q = \beta_q = \frac{1}{2}$, corresponding to the contribution from left-handed quarks. The results are plotted in Fig 15. From the figures, we see that a signal at current generation neutrino telescopes implies that the masses of the colored fermions lie at a TeV or below, which is within the kinematic reach of the LHC.

4. Conclusions

In conclusion we have used the constraints from direct detection experiments to establish a model-independent upper bound on dark matter event rates in neutrino telescopes, which applies to any elastic dark matter model. The strength of the bound depends on whether the WIMP-nucleon cross section is spin-independent or spin-dependent. While the spin-dependent bound is not competitive with present limits from neutrino telescopes, the spin-independent bound is much tighter, and is comparable to current experimental bounds. As direct detection experiments improve, these bounds are expected to get even tighter.

If the observed event rate in neutrino telescopes exceeds the bound corresponding to spin-independent interactions, we can immediately infer that WIMP-nucleon scattering is dominated by spin-dependent interactions. The dark matter candidates that naturally have this property have been classified, and are known to be either Majorana fermions or real vector bosons, so that the dark matter particle is its own anti-particle. Furthermore, it is

known that each such candidate theory predicts either new particles at the weak scale with SM quantum numbers, or a new Z' gauge boson with mass close to the weak scale. We have studied the parameter space of these theories which leads to an observable signal at IceCube, and found that while the scenario with a new Z' gauge boson is somewhat disfavored by current experimental constraints, the alternate scenario is completely viable. The masses of the new particles are favored to lie at energy scales that are kinematically accessible to the LHC.

Acknowledgments

We would like to thank Lian-Tao Wang for comments. PA, ZC and RKM are supported by the National Science Foundation under grant number PHY-0801323. CK is supported by the Department of Energy under grant DE-FG0296ER50959.

References

- [1] J. R. Ellis, J. S. Hagelin, D. V. Nanopoulos, K. A. Olive, and M. Srednicki, *Supersymmetric relics from the big bang*, *Nucl. Phys.* **B238** (1984) 453–476.
- [2] K. Griest, *Cross sections, relic abundance, and detection rates for neutralino dark matter*, *Phys. Rev.* **D38** (1988) 2357.
- [3] E. W. Kolb and R. Slansky, *Dimensional Reduction in the Early Universe: Where Have the Massive Particles Gone?*, *Phys. Lett.* **B135** (1984) 378.
- [4] G. Servant and T. M. P. Tait, *Is the lightest Kaluza-Klein particle a viable dark matter candidate?*, *Nucl. Phys.* **B650** (2003) 391–419, [[hep-ph/0206071](#)].
- [5] A. Birkedal-Hansen and J. G. Wacker, *Scalar dark matter from theory space*, *Phys. Rev.* **D69** (2004) 065022, [[hep-ph/0306161](#)].
- [6] J. Hubisz and P. Meade, *Phenomenology of the littlest Higgs with T-parity*, *Phys. Rev.* **D71** (2005) 035016, [[hep-ph/0411264](#)].
- [7] A. Birkedal, A. Noble, M. Perelstein, and A. Spray, *Little Higgs dark matter*, *Phys. Rev.* **D74** (2006) 035002, [[hep-ph/0603077](#)].
- [8] E. M. Dolle and S. Su, *Dark Matter in the Left Right Twin Higgs Model*, *Phys. Rev.* **D77** (2008) 075013, [[arXiv:0712.1234](#)].
- [9] J. Silk, K. A. Olive, and M. Srednicki, *The photino, the sun, and high-energy neutrinos*, *Phys. Rev. Lett.* **55** (1985) 257–259.
- [10] M. Srednicki, K. A. Olive, and J. Silk, *High-Energy Neutrinos from the Sun and Cold Dark Matter*, *Nucl. Phys.* **B279** (1987) 804.
- [11] L. Bergstrom, J. Edsjo, and P. Gondolo, *Indirect neutralino detection rates in neutrino telescopes*, *Phys. Rev.* **D55** (1997) 1765–1770, [[hep-ph/9607237](#)].
- [12] L. Bergstrom, J. Edsjo, and P. Gondolo, *Indirect detection of dark matter in km-size neutrino telescopes*, *Phys. Rev.* **D58** (1998) 103519, [[hep-ph/9806293](#)].

- [13] V. D. Barger, F. Halzen, D. Hooper, and C. Kao, *Indirect search for neutralino dark matter with high energy neutrinos*, *Phys. Rev.* **D65** (2002) 075022, [[hep-ph/0105182](#)].
- [14] V. Barger, W.-Y. Keung, G. Shaughnessy, and A. Tregre, *High energy neutrinos from neutralino annihilations in the Sun*, *Phys. Rev.* **D76** (2007) 095008, [[arXiv:0708.1325](#)].
- [15] V. Bertin, E. Nezri, and J. Orloff, *Neutrino indirect detection of neutralino dark matter in the CMSSM*, *Eur. Phys. J.* **C26** (2002) 111–124, [[hep-ph/0204135](#)].
- [16] V. Bertin, E. Nezri, and J. Orloff, *Neutralino dark matter beyond CMSSM universality*, *JHEP* **02** (2003) 046, [[hep-ph/0210034](#)].
- [17] D. Hooper and L.-T. Wang, *Direct and indirect detection of neutralino dark matter in selected supersymmetry breaking scenarios*, *Phys. Rev.* **D69** (2004) 035001, [[hep-ph/0309036](#)].
- [18] G. Jungman, M. Kamionkowski, and K. Griest, *Supersymmetric dark matter*, *Phys. Rept.* **267** (1996) 195–373, [[hep-ph/9506380](#)].
- [19] H.-C. Cheng, J. L. Feng, and K. T. Matchev, *Kaluza-Klein dark matter*, *Phys. Rev. Lett.* **89** (2002) 211301, [[hep-ph/0207125](#)].
- [20] D. Hooper and G. D. Kribs, *Probing Kaluza-Klein dark matter with neutrino telescopes*, *Phys. Rev.* **D67** (2003) 055003, [[hep-ph/0208261](#)].
- [21] B. A. Dobrescu, D. Hooper, K. Kong, and R. Mahbubani, *Spinless photon dark matter from two universal extra dimensions*, *JCAP* **0710** (2007) 012, [[arXiv:0706.3409](#)].
- [22] M. Blennow, H. Melbeus, and T. Ohlsson, *Neutrinos from Kaluza-Klein dark matter in the Sun*, [arXiv:0910.1588](#).
- [23] T. Flacke, A. Menon, D. Hooper, and K. Freese, *Kaluza-Klein Dark Matter And Neutrinos From Annihilation In The Sun*, [arXiv:0908.0899](#).
- [24] D. Hooper and G. Servant, *Indirect detection of Dirac right-handed neutrino dark matter*, *Astropart. Phys.* **24** (2005) 231–246, [[hep-ph/0502247](#)].
- [25] M. Perelstein and A. Spray, *Indirect detection of little Higgs dark matter*, *Phys. Rev.* **D75** (2007) 083519, [[hep-ph/0610357](#)].
- [26] P. Agrawal, E. M. Dolle, and C. A. Krenke, *Signals of Inert Doublet Dark Matter in Neutrino Telescopes*, *Phys. Rev.* **D79** (2009) 015015, [[arXiv:0811.1798](#)].
- [27] S. Andreas, M. H. G. Tytgat, and Q. Swillens, *Neutrinos from Inert Doublet Dark Matter*, *JCAP* **0904** (2009) 004, [[arXiv:0901.1750](#)].
- [28] S. Andreas, *Neutrino signature of Inert Doublet Dark Matter*, [arXiv:0911.0540](#).
- [29] R. Allahverdi, S. Bornhauser, B. Dutta, and K. Richardson-McDaniel, *Prospects for Indirect Detection of Sneutrino Dark Matter with IceCube*, *Phys. Rev.* **D80** (2009) 055026, [[arXiv:0907.1486](#)].
- [30] M. Kamionkowski, K. Griest, G. Jungman, and B. Sadoulet, *Model independent comparison of direct versus indirect detection of supersymmetric dark matter*, *Phys. Rev. Lett.* **74** (1995) 5174–5177, [[hep-ph/9412213](#)].

[31] F. Halzen and D. Hooper, *Prospects for detecting dark matter with neutrino telescopes in light of recent results from direct detection experiments*, *Phys. Rev.* **D73** (2006) 123507, [[hep-ph/0510048](#)].

[32] G. Wikstrom and J. Edsjo, *Limits on the WIMP-nucleon scattering cross-section from neutrino telescopes*, *JCAP* **0904** (2009) 009, [[arXiv:0903.2986](#)].

[33] A. Bandyopadhyay, S. Chakraborty, and D. Majumdar, *Interpreting the bounds on Dark Matter induced muons at Super-Kamiokande in the light of CDMS data*, [arXiv:1002.0753](#).

[34] **IceCube** Collaboration, R. Abbasi *et. al.*, *Limits on a muon flux from neutralino annihilations in the Sun with the IceCube 22-string detector*, *Phys. Rev. Lett.* **102** (2009) 201302, [[arXiv:0902.2460](#)].

[35] **IceCube** Collaboration, . R. Abbasi, *Limits on a muon flux from Kaluza-Klein dark matter annihilations in the Sun from the IceCube 22-string detector*, [arXiv:0910.4480](#).

[36] P. Agrawal, Z. Chacko, C. Kilic, and R. K. Mishra, *Direct Detection Constraints on Dark Matter Event Rates in Neutrino Telescopes, and Collider Implications*, [arXiv:1003.1912](#).

[37] **The CDMS-II** Collaboration, Z. Ahmed *et. al.*, *Results from the Final Exposure of the CDMS II Experiment*, [arXiv:0912.3592](#).

[38] J. Angle *et. al.*, *Limits on spin-dependent WIMP-nucleon cross-sections from the XENON10 experiment*, *Phys. Rev. Lett.* **101** (2008) 091301, [[arXiv:0805.2939](#)].

[39] S. Archambault *et. al.*, *Dark Matter Spin-Dependent Limits for WIMP Interactions on 19-F by PICASSO*, *Phys. Lett.* **B682** (2009) 185–192, [[arXiv:0907.0307](#)].

[40] **KIMS** Collaboration, S. K. Kim, *New results from the KIMS experiment*, *J. Phys. Conf. Ser.* **120** (2008) 042021.

[41] A. Gould, *Cosmological density of WIMPs from solar and terrestrial annihilations*, *Astrophys. J.* **388** (1992) 338–344.

[42] P. Gondolo *et. al.*, *DarkSUSY: Computing supersymmetric dark matter properties numerically*, *JCAP* **0407** (2004) 008, [[astro-ph/0406204](#)].

[43] S. I. Dutta, M. H. Reno, I. Sarcevic, and D. Seckel, *Propagation of muons and taus at high energies*, *Phys. Rev.* **D63** (2001) 094020, [[hep-ph/0012350](#)].

[44] R. Gandhi, C. Quigg, M. H. Reno, and I. Sarcevic, *Ultrahigh-energy neutrino interactions*, *Astropart. Phys.* **5** (1996) 81–110, [[hep-ph/9512364](#)].

[45] J. Kopp, V. Niro, T. Schwetz, and J. Zupan, *DAMA/LIBRA and leptonically interacting Dark Matter*, *Phys. Rev.* **D80** (2009) 083502, [[arXiv:0907.3159](#)].

[46] E. Aprile, *The XENON100 dark matter experiment*, *AIP Conf. Proc.* **1115** (2009) 355–360.

[47] S. Fiorucci *et. al.*, *Status of the LUX Dark Matter Search*, [arXiv:0912.0482](#).

[48] **Super-Kamiokande** Collaboration, S. Desai *et. al.*, *Study of TeV Neutrinos with Upward Showering Muons in Super-Kamiokande*, *Astropart. Phys.* **29** (2008) 42–54, [[arXiv:0711.0053](#)].

[49] **IceCube** Collaboration, C. de Clercq, *Search for Dark Matter with the AMANDA and IceCube neutrino detectors (20'+5')*, in *Identification of dark matter*, 2008.

[50] A. Sommerfeld, *ber die Beugung und Bremsung der Elektronen*, *Annalen der Physik* **403** (1931), no. 3 257–330.

[51] M. Cirelli, A. Strumia, and M. Tamburini, *Cosmology and Astrophysics of Minimal Dark Matter*, *Nucl. Phys.* **B787** (2007) 152–175, [[arXiv:0706.4071](#)].

[52] N. Arkani-Hamed, D. P. Finkbeiner, T. R. Slatyer, and N. Weiner, *A Theory of Dark Matter*, *Phys. Rev.* **D79** (2009) 015014, [[arXiv:0810.0713](#)].

[53] P. F. Bedaque, M. I. Buchoff, and R. K. Mishra, *Sommerfeld enhancement from Goldstone pseudo-scalar exchange*, *JHEP* **11** (2009) 046, [[arXiv:0907.0235](#)].

[54] D. Tucker-Smith and N. Weiner, *Inelastic dark matter*, *Phys. Rev.* **D64** (2001) 043502, [[hep-ph/0101138](#)].

[55] D. Tucker-Smith and N. Weiner, *The status of inelastic dark matter*, *Phys. Rev.* **D72** (2005) 063509, [[hep-ph/0402065](#)].

[56] Y. Cui, D. E. Morrissey, D. Poland, and L. Randall, *Candidates for Inelastic Dark Matter*, *JHEP* **05** (2009) 076, [[arXiv:0901.0557](#)].

[57] B. Feldstein, A. L. Fitzpatrick, and E. Katz, *Form Factor Dark Matter*, [arXiv:0908.2991](#).

[58] S. Chang, A. Pierce, and N. Weiner, *Momentum Dependent Dark Matter Scattering*, [arXiv:0908.3192](#).

[59] Y. Bai and P. J. Fox, *Resonant Dark Matter*, *JHEP* **11** (2009) 052, [[arXiv:0909.2900](#)].

[60] S. Nussinov, L.-T. Wang, and I. Yavin, *Capture of Inelastic Dark Matter in the Sun*, *JCAP* **0908** (2009) 037, [[arXiv:0905.1333](#)].

[61] A. Menon, R. Morris, A. Pierce, and N. Weiner, *Capture and Indirect Detection of Inelastic Dark Matter*, [arXiv:0905.1847](#).

[62] J. R. Ellis, A. Ferstl, and K. A. Olive, *Re-evaluation of the elastic scattering of supersymmetric dark matter*, *Phys. Lett.* **B481** (2000) 304–314, [[hep-ph/0001005](#)].

[63] G. K. Mallot, *The spin structure of the nucleon*, [hep-ex/9912040](#).

[64] T. Cohen, D. J. Phalen, and A. Pierce, *On the Correlation Between the Spin-Independent and Spin- Dependent Direct Detection of Dark Matter*, [arXiv:1001.3408](#).

[65] T. Appelquist, B. A. Dobrescu, and A. R. Hopper, *Nonexotic neutral gauge bosons*, *Phys. Rev.* **D68** (2003) 035012, [[hep-ph/0212073](#)].

[66] **Particle Data Group** Collaboration, C. Amsler *et. al.*, *Review of particle physics*, *Phys. Lett.* **B667** (2008) 1.

[67] J. Alwall, M.-P. Le, M. Lisanti, and J. G. Wacker, *Model-Independent Jets plus Missing Energy Searches*, *Phys. Rev.* **D79** (2009) 015005, [[arXiv:0809.3264](#)].

[68] E. Izaguirre, M. Manhart, and J. G. Wacker, *Bigger, Better, Faster, More at the LHC*, [arXiv:1003.3886](#).

[69] Q.-H. Cao, C.-R. Chen, C. S. Li, and H. Zhang, *Effective Dark Matter Model: Relic density, CDMS II, Fermi LAT and LHC*, [arXiv:0912.4511](#).

[70] M. Beltran, D. Hooper, E. W. Kolb, Z. A. C. Krusberg, and T. M. P. Tait, *Maverick dark matter at colliders*, [arXiv:1002.4137](#).